The 2023 World Congress on
Advances in Structural Engineering and Mechanics (ASEM23)
GECE, Seoul, Korea, August 16-18, 2023

PDMS-embedded Fiber Grating curvature sensor for displacement measurement applications

*Fernando Velazquez-Carreon[1)], Abraham Perez-Alonzo[2)], G.E. Sandoval-Romero[3)], Celia Sanchez-Perez[4)]

[1), 2),3),4)] *Instituto de Ciencias Aplicadas y Tecnología, Universidad Nacional Autónoma de México, Ciudad de México 04510, México*

[*] fvelazqu@ciencias.unam.mx

ABSTRACT

In this study, we present a curvature sensor that utilizes Fiber Bragg Gratings (FBG) embedded in Polydimethylsiloxane polymer (PDMS) to measure displacement accurately. These embedded sensors offer high sensitivity to measurement of pressure, temperature, and deformation due to the unique mechanical characteristics of PDMS. Traditionally, FBG-based curvature sensors have found applications in Structural Health Monitoring, aerospace engineering, and robotics, where changes in curvature cause a shift in the Bragg wavelength reflected.

Our sensors proposal can measure both tensile and compressive strain of the Bragg gratings, depending on the direction of displacement with a high sensitivity comparing with a non-embedded FBG sensor. To validate their performance, we conducted finite element analysis simulations using Ansys software and compared the results with experimental data. Our experiments involved both a solid structure and a modified hollow structure with three central perforations, designed to increase the sensor's sensitivity to curvature variations.

The two prototype sensors exhibited displacement sensitivities of 110 pm/mm and 128 pm/mm in cases of tension deformation, and -116 pm/mm and -118 pm/mm in cases of compression. Notably, the structure with perforations demonstrated a 15% increase in sensitivity compared to the homogeneous structure.

Overall, this novel curvature sensor design presents promising potential for precise displacement measurement in various fields, leveraging the advantages of FBG technology and PDMS characteristics.

---

[1] Ph.D. candidate
[2] Ph.D. candidate
[3] Professor
[4] Professor

1. INTRODUCTION

In recent years, fiber optic sensors have gained prominence in Structural Health Monitoring (SHM) applications due to their numerous advantages, such as high sensitivity, immunity to electromagnetic interference, and remote sensing capabilities (Elsherif, 2022).

Fiber Bragg Grating (FBG) sensors, in particular, have proven to be highly versatile, capable of measuring deformations, curvatures, displacements, pressure, and temperature changes. These attributes make them an ideal choice for developing remote sensing systems used in Structural Health Monitoring (SHM) (Mousumi, 2022).

FBG sensors consist of micro modulations in the fiber optic core, as illustrated in Fig.1. These modulations result in a specific wavelength being reflected, which can be used for various sensing purposes, given by:

$$\lambda_b = 2n_{eff}\Lambda \tag{1}$$

Where λ_b is the reflected Bragg wavelength, n_{eff} is the effective index refraction of the fiber optic core and Λ is the grating period. The Bragg wavelength is shifted ($\Delta\lambda_b$) in response to axial deformations (ϵ) or temperature variations (ΔT) of the Bragg grating in a fiber optic sensor, that can be expressed using the following equation:

$$\frac{\Delta\lambda_b}{\lambda_b} = (1 - p_e)\epsilon + (\eta + \alpha)\Delta T \tag{2}$$

$\Delta\lambda_b$ is the wavelength shift of λ_b, p_e is the photo-elastic coefficient of the fiber, ϵ is the axial strain (deformation) applied to the fiber, α is the thermal expansion coefficient of FBG, η is the thermo-optic coefficient of FBG. For a silica-based fiber, the constant values are: $p_e \simeq 0.22$, $\alpha \simeq 0.55\times10^{-6}$/°C, and $\eta \simeq 8.61\times10^{-6}$/°C (Bashir 2006).

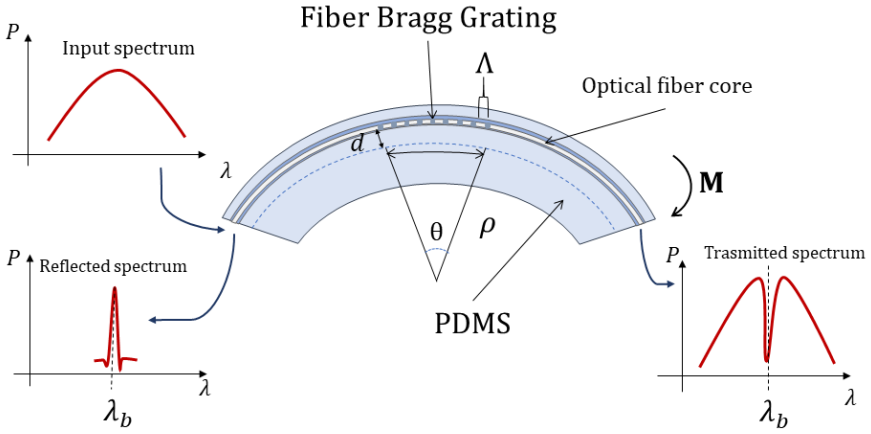

Fig. 1 Diagram of the PDMS-FBG embedded sensor subject to curvature changes due to bending moment **M**.

This formula allows researchers and engineers to quantify the wavelength shift, which serves as the basis for measuring and monitoring the applied strain or temperature variations in the fiber optic sensor.

Polymer embedded Fiber Bragg Grating (FBG) sensors have gained popularity due to their ability to shield the optical fiber from environmental effects while providing increased sensitivity to deformations and temperature changes.

Among the various polymer options, Polydimethylsiloxane (PDMS) has emerged as a preferred material for encapsulating FBG sensors. PDMS is advantageous for several reasons: it is non-toxic, exhibits resistance to UV radiation, is electrically non-conductive, and does not interfere with the proper functioning of the FBG. Moreover, PDMS offers the flexibility to control the deformation experienced by the FBG, depending on the geometry of the PDMS used.

These embedded sensors have found application in diverse fields, such as:

1. **Vehicle Traffic Monitoring** (Falkus, 2020): PDMS-embedded FBG sensors have been utilized to monitor traffic conditions on roads and highways. The sensors can detect and measure changes in road surface conditions, providing valuable data for traffic management and road maintenance.
2. **Water Volume Control in Tanks** (Morais, 2022): By employing PDMS-embedded FBG sensors, water levels in tanks can be accurately monitored. The sensors offer precise measurements and reliable feedback for managing water resources efficiently.
3. **Heart Rate Monitoring** (Nedoma, 2017): In the medical field, PDMS-embedded FBG sensors have been used for non-invasive heart rate monitoring. Placed on the skin, these sensors detect subtle changes in blood flow, providing real-time heart rate information without the need for invasive procedures.

Overall, the versatility and performance of polymer embedded FBG sensors, particularly using PDMS as the encapsulating material, have opened up numerous possibilities for a wide range of applications, enhancing our ability to monitor and analyze various parameters in a non-intrusive and reliable manner.

The measurement of linear displacements by means of curvature variations have already been proposed previously, these sensors deform the Bragg grating when the radius of curvature of the structure to which it is attached changes. In this way, the deformation of the Bragg grating can be written as, $\epsilon = d/\rho$, where d is the distance to neutral axis to center of the FBG, and ρ is the radius of curvature shown in the Fig. 1. These sensors are used because of the linearity of the deformation response, i.e., the wavelength shift of λ_b, the high sensitivity and the measuring range, which can be determined according to the dimensions of the sensor.

From this, two embedded PDMS-FBG structures for displacement and curvature monitoring were developed for possible structural monitoring applications. The concept of measuring linear displacements through curvature variations has been previously proposed by our research group (Velazquez-Carreon 2023).

In this work upon these advantages, two PDMS-embedded FBG devices were developed for displacement and curvature monitoring. These devices hold significant

potential for SHM applications, offering reliable and accurate data for assessing the integrity and performance of several structures.

2. CURVATURE-DISPLACEMENT SENSING PRINCIPLE

Devices based on PDMS-embedded Bragg gratings was fabricated, at the ends subject to trapezoidal structures to induce curvature changes in the bending zone, one end being fixed and the other free from displacement (Δx). For the calculation of the curvature of the developed structure, the following geometrical relationship can be used (Wang 2018).

$$C = \frac{1}{R} = \frac{2h}{h^2 + D^2} \tag{3}$$

Where C is the curvature, R is the bending curvature radius, D is the half of the distance between the end points of the bending zone, and h is the height of the bending displacement.

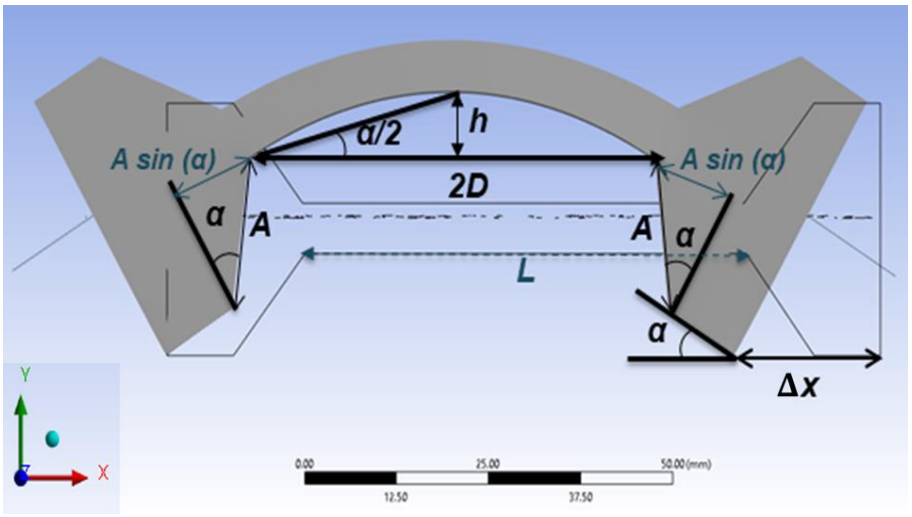

Fig. 2 Curvature-displacement sensing diagram

According to Fig. 2, to estimate the curvature of the structure due to linear displacements only in the x-axis, the following data were used. For the distance $2D$ we consider the initial length of the structure L, the angle formed by the linear displacement α, the length A from base to bending area. And the distance traveled by one end of the structure Δx, represented by the following equation:

$$2D = L + 2A\ sen\ \alpha - \Delta x \tag{4}$$

The bending height h caused by linear displacements, is determined considering the distance D, and the sine of the angle $\alpha/2$,

$$h = \left(\frac{L + 2A\ sen\ \alpha - \Delta x}{2}\right) sen\frac{\alpha}{2} \tag{5}$$

Combining Eq. (4) and Eq. (5) in the curvature geometric relationship, we obtain a curvature-displacement relation by the form:

$$C = \frac{2\left(\left(\frac{L + 2A\ sen\ \alpha - \Delta x}{2}\right) sen\frac{\alpha}{2}\right)}{\left(\left(\frac{L + 2A\ sen\ \alpha - \Delta x}{2}\right) sen\frac{\alpha}{2}\right)^2 + \left(\frac{L + 2A\ sen\ \alpha - \Delta x}{2}\right)^2} \tag{6}$$

Considering a constant temperature in the FBG, Eq. (2) the Bragg wavelength shift can be simplify in the form:

$$\frac{\Delta\lambda_b}{\lambda_b} = (1 - p_e)\epsilon \tag{7}$$

For a strain by bending, the axial-strain is in the form $\epsilon = Cd$, where d is the distance to neutral axis to center of the FBG, combining this strain in the Eq. (7), we have a wavelength shift $\Delta\lambda_b$ in terms of curvature variations in the form:

$$\frac{\Delta\lambda_b}{\lambda_b} = (1 - p_e)Cd \tag{8}$$

Substituting the curvature displacement equation Eq. (6) in the wavelength shift equation Eq. (7) we have the following equation:

$$\Delta\lambda_b = \lambda_b(1 - p_e)\left(\frac{2\left(\left(\frac{L + 2A\ sen\ \alpha - \Delta x}{2}\right) sen\frac{\alpha}{2}\right)}{\left(\left(\frac{L + 2A\ sen\ \alpha - \Delta x}{2}\right) sen\frac{\alpha}{2}\right)^2 + \left(\frac{L + 2A\ sen\ \alpha - \Delta x}{2}\right)^2}\right) d \tag{9}$$

In this way, it is possible to geometrically estimate the $\Delta\lambda_b$ of our FBG sensor due to curvature changes induced by linear displacements.

3. STRAIN-ANALYSIS FEM SIMULATION

A finite element method (FEM) simulation was performed using Ansys software to study the deformation of the PDMS structure and the fiber optic Bragg grating when subjected to curvature changes resulting from linear displacements. The simulation aimed to replicate the experimental conditions and obtain valuable information about the behavior of both the solid structure and the hollow structure with three central perforations, according to the dimensions shown in Fig. 3.

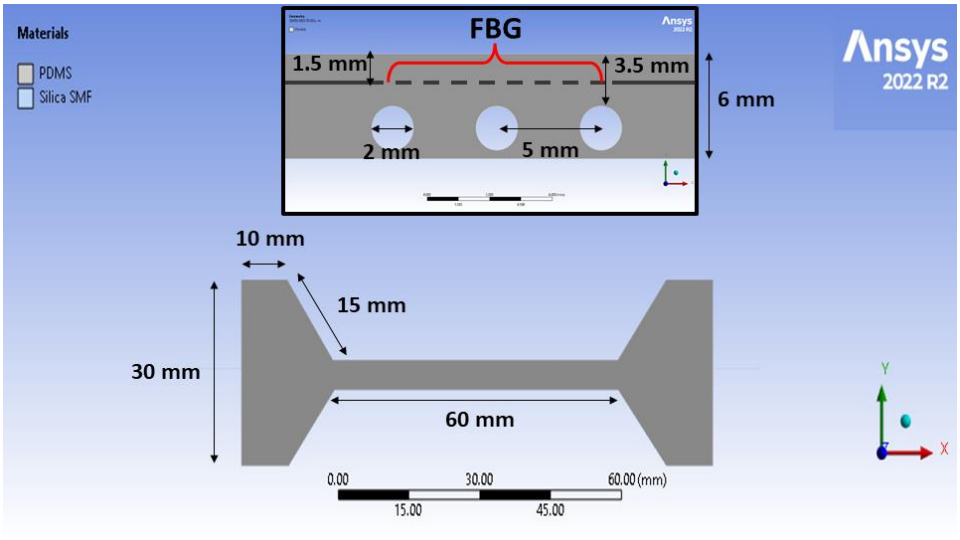

Fig. 3 Dimensions of the solid PDMS-embedded fiber grating sensor, showing also the dimensions of the aligned perforations of the hollow device.

To carry out the deformation simulation, the parameters of the mechanical properties of the materials used, shown in Tab.1.

Tab.1. Mechanical properties of the materials used

Material	Density	Young Modulus	Poisson ratio
PDMS (Ariati 2021)	0.97 g/cm^3	1.35 MPa	0.49
Silica SMF (Lakshmanan 2022)	2.19 g/cm^3	73 GPa	0.17

The simulation consisted in determining the deformation of the silica Single-mode fiber (SMF) embedded in the central part of the PDMS device by means of curvature changes due to linear displacements Δx, with the purpose to estimate the deformation of the FBG in the central part of the bending zone, and determine $\Delta\lambda_b$ resulting from axial deformations.

Two devices with identical dimensions were simulated, as shown in Fig. 4. The only difference between them is that one of the structures contains three central holes

located beneath the embedded FBG. The purpose of adding these holes is to estimate the change in the deformation of the FBG resulting from the concentration of stresses in the structure subjected to bending deformation (Pilkey 2005).

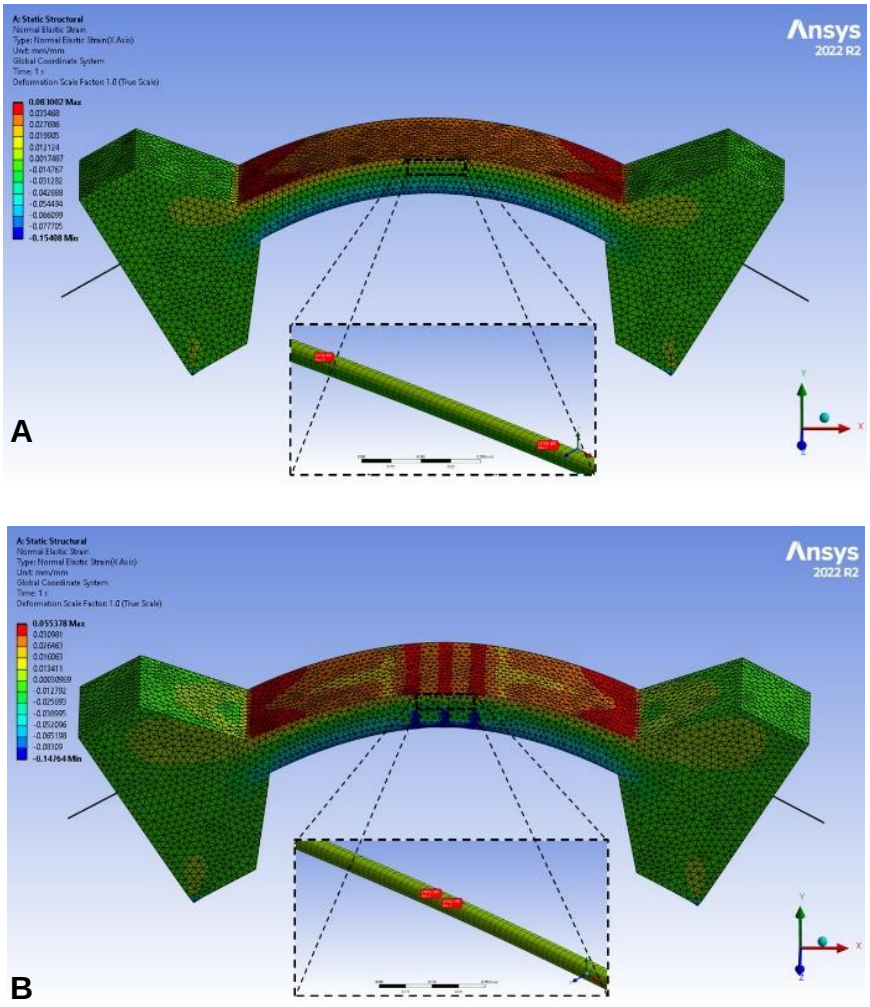

Fig. 4 FEM simulation of strain in the PDMS-FBG sensor by curvature variations, **A)** Solid structure, **B)** Structure with three central holes.

Depending on the position of the FBG within the PDMS structure, it will experience either tension or compression deformations. These deformations result from its relative location with respect to the neutral plane. When the FBG is positioned above the neutral plane, it undergoes tension, whereas if it is below the neutral plane, it experiences compression. This positional change can be achieved by rotating the structure 180 degrees around the X-axis.

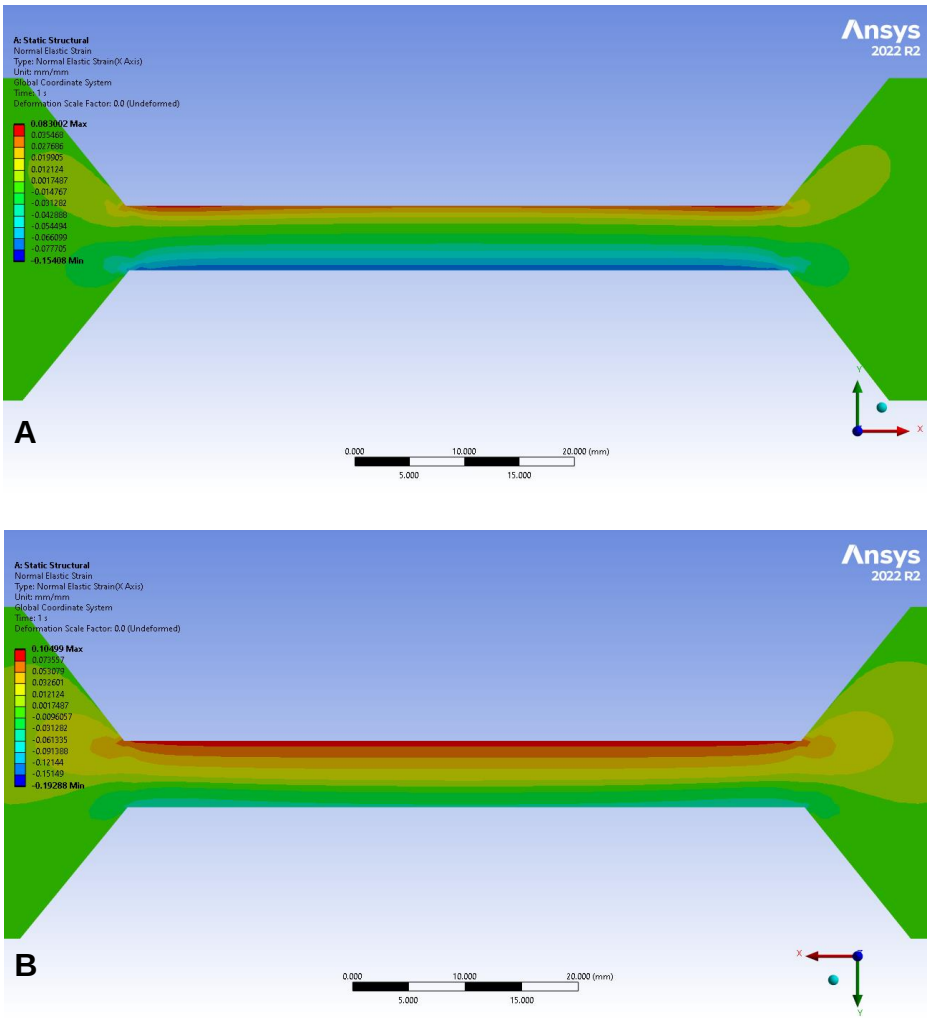

Fig. 5 FEM simulation of strain in the PDMS-FBG solid sensor, A) FBG in strain tension zone upper the neutral axis, B) FBG in strain compression zone under the neutral axis

The tension and compression zones for each case are illustrated in Fig. 5. In Fig. 5A, the original position of the optical fiber with the embedded FBG is located in the upper zone, where mechanical tensile strain occurs due to deformation. On the other hand, Fig. 5B shows the structure rotated 180 degrees, with the fiber and grating now positioned in the zones where compression strain acts. This change is achieved by applying the same displacement along the X-axis.

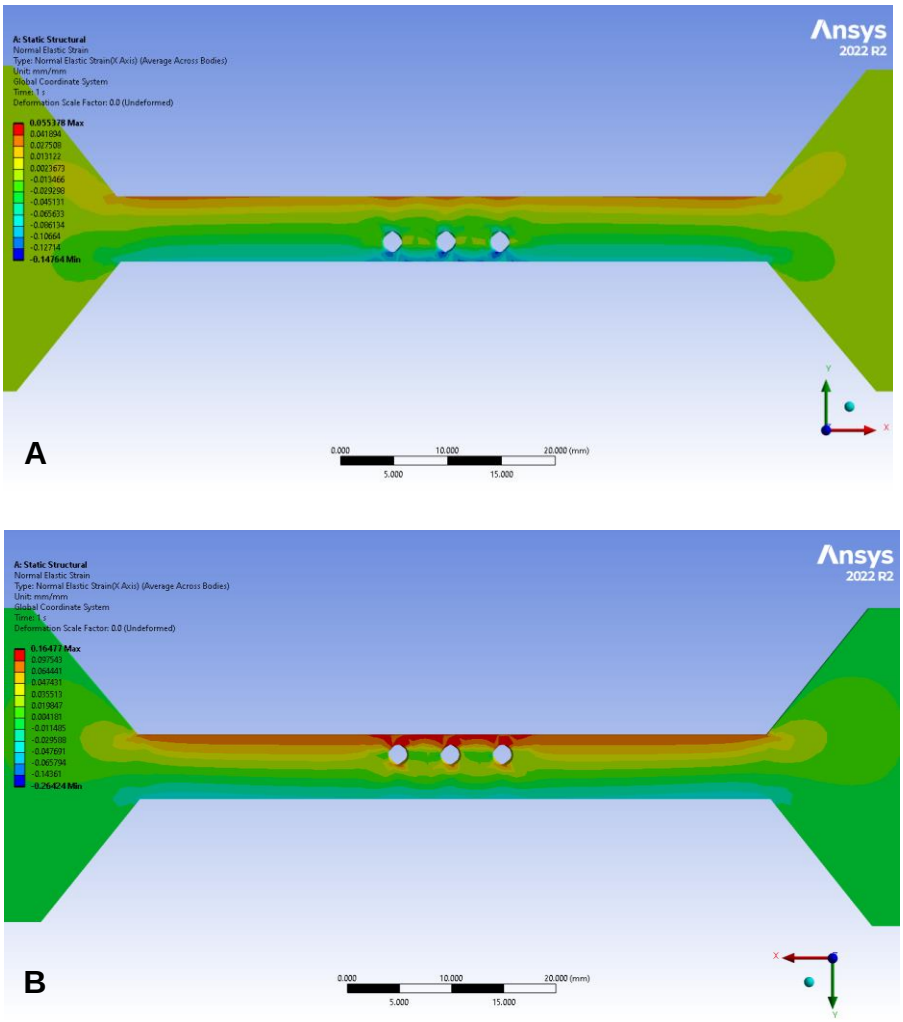

Fig. 6 FEM simulation of strain in the perforated PDMS-FBG sensor, **A)** FBG in strain tension zone upper the neutral axis, **B)** FBG in strain compression zone under the neutral axis

This behavior is also observed in the hollow device in the central bending zone, as shown in Fig. 6. In this case, the phenomenon of strain concentration becomes apparently, where the strain planes experience compaction. As a result, there is an increase in the deformation suffered by the device in this zone, affecting the FBG embedded in this location.

These results are crucial in estimating the deformation of the embedded FBG and its sensitivity to deformations under linear displacements in both cases. Furthermore, they are compared with the experimental situation, where the devices undergo tensile and compressive forces due to variations in curvature.

4. PDMS-EMBEDDED DEVICES FABRICATION AND TESTING

To fabricate these structures, a removable mold was created using a 3D printer with PLA plastic infused with carbon fiber. The mold was then secured to a metal square plate to provide additional support. An FBG from the manufacturer Alxenses, with a wavelength of λ_b=1529.750 nm, was attached to the ends of the mold. This was achieved by applying pressure and fastening it with screws to ensure tautness during the PDMS curing process.

Sylgard 184 PDMS was mixed in a 10:1 ratio and used to fill the mold. The entire mold was then placed in a vacuum chamber to remove bubbles from the PDMS for 15 minutes, as shown in Fig. 6A, with intervals of 5 minutes.

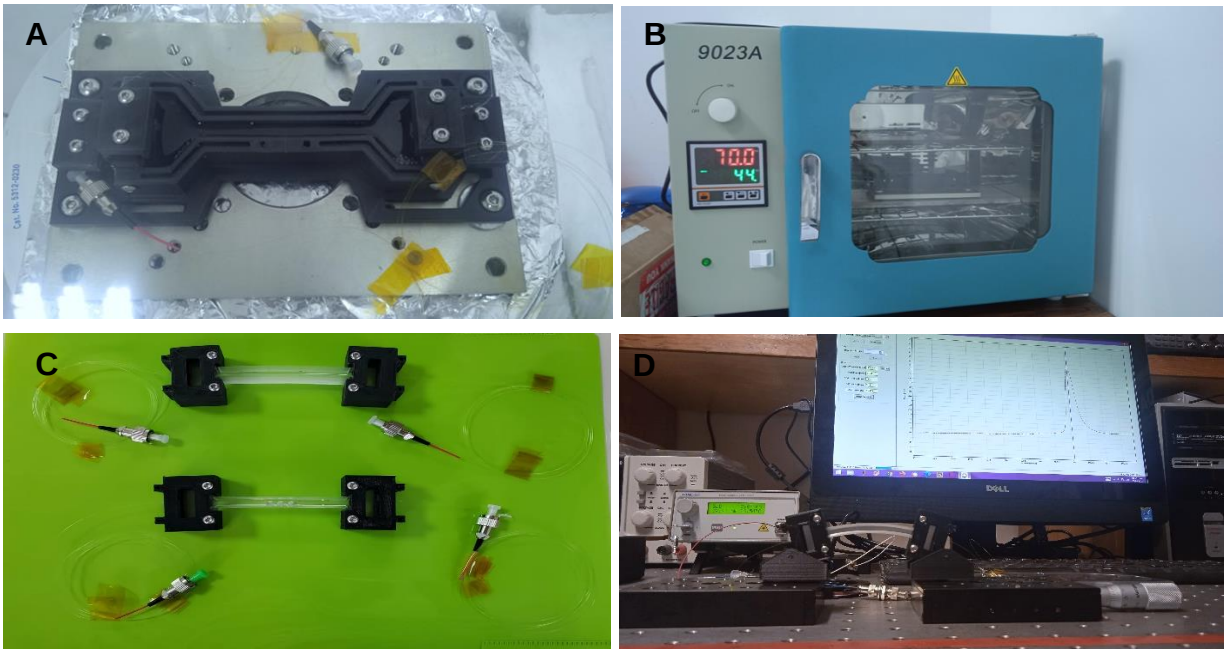

Fig. 7 Fabrication and testing PDMS-FBG devices. **A)** 3D printing mold in vacuum chamber, **B)** Curing process into the oven to 70°C, **C)** PDMS-FBG embedded devices demolded, **D)** Sensors with lateral displacement supports,

After filling the mold with PDMS and the embedded FBG, the structure was placed in an oven to initiate the curing process, as shown in Fig. 7B. The curing temperature was set to 70 °C, and the mold was kept in the oven for 120 minutes.

Once the curing time elapsed, the structure was demolded (Fig. 7C) and left to cool to ambient temperature to prevent any damage to the PDMS.

Lateral supports, also made with 3D printing, were placed on the finished structures to induce changes in curvature through linear displacements. The structure was positioned on two micrometric plates to apply controlled displacements (Fig. 7D). This allowed us to monitor the displacement of the wavelength of the immersed Bragg grating before and after the changes in curvature caused by linear displacements.

For wavelength shift monitoring, the Bragg grating was connected to an optical circulator, which is fed by an Thorlabs SLD (Super Luminescent Source), and the

reflected spectrum is measured by an Fiberer OSA (Optical Spectrum Analyzer) with a resolution of 2 picometers connected to a PC, as shown in Fig. 8.

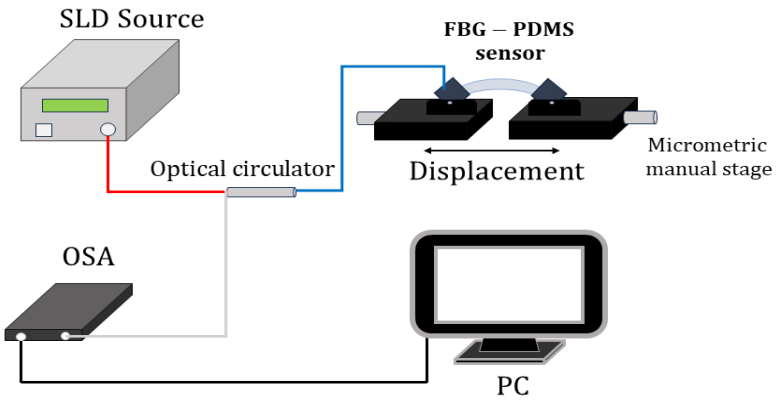

Fig. 8 Experimental set up diagram for the measurement of the Bragg wavelength shift to curvature sensor by linear displacements.

For both devices (Fig. 9), the characterization was conducted within the same range of displacement, from 0 to 20 mm, considering both tensile and compressive positions of the FBG. The variation of curvature of the structure was measured, along with the response of the embedded Bragg grating to temperature changes within a range of 20 to 52 °C.

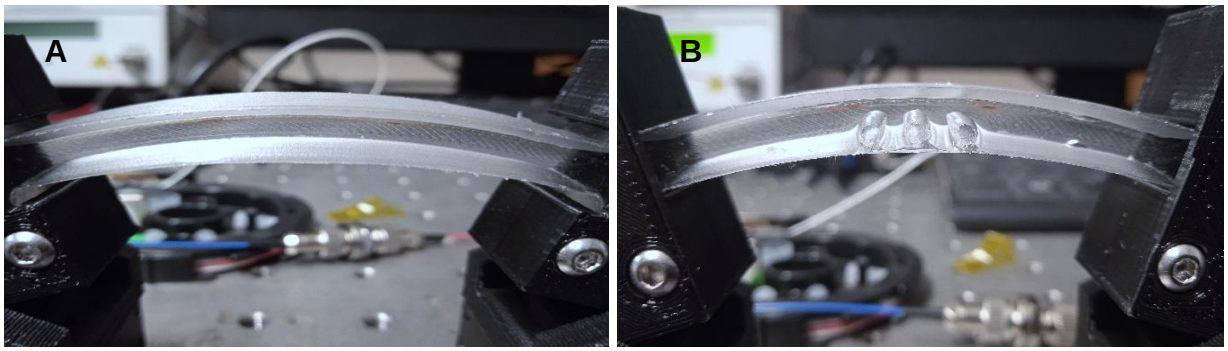

Fig. 9 PDMS-FBG embedded sensor under curvature variations, **A)** Solid structure**,** **B)** Hollow structure.

5. TEST RESULTS AND DISCUSSION

First, the strain response of the Bragg grating due to curvature changes in linear displacements for both tension and compression of the grating was obtained, with a

range of 0 to 20 mm. Then, the experimental data were compared with the results obtained from the simulations using the Ansys software in addition to those calculated from the equation Eq. (9).

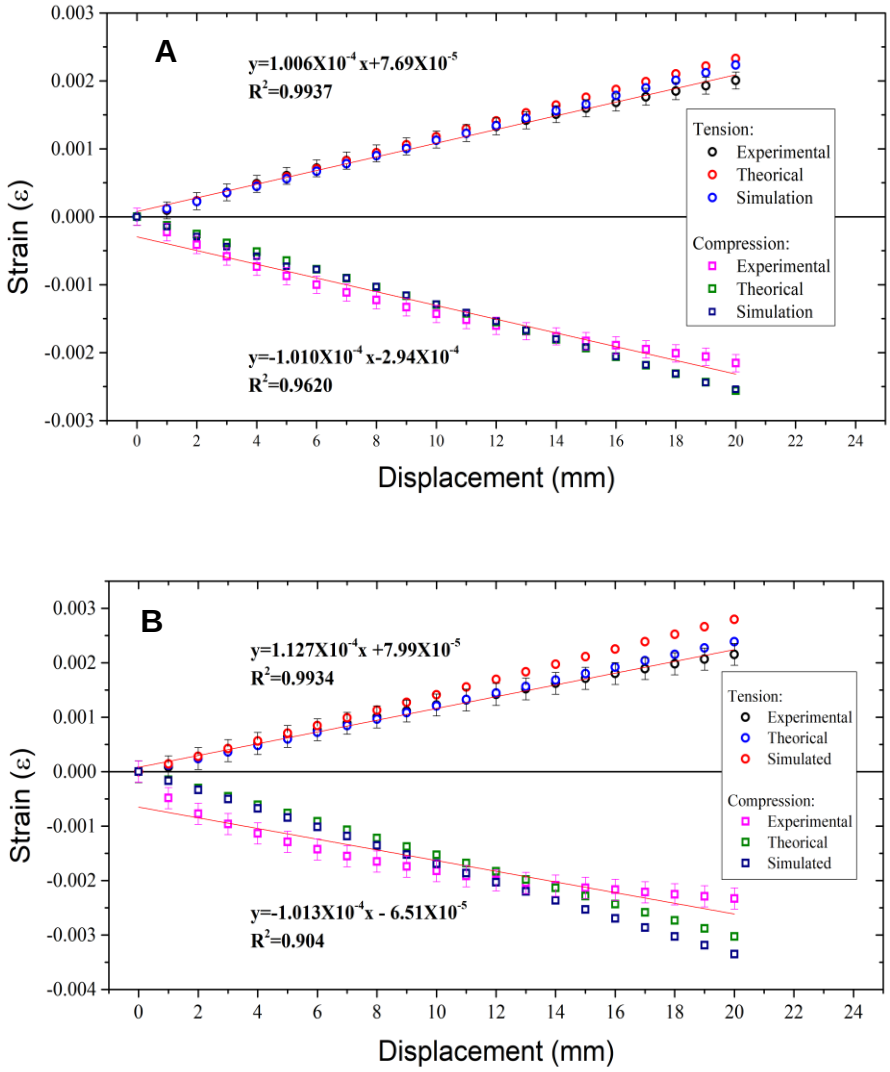

Fig. 10 Comparison of the FBG strain of the theoretical, simulated and experimental data with linear fit, **A)** Solid device, **B)** Hollow device

For the case of the solid device (Fig. 10A), the deformation under tension shows a high similarity between the experimental, theoretical, and simulated data. However, small discrepancies start to appear from 15 mm of displacement, causing a reduction in the linear tendency of strain by displacement. This discrepancy might be attributed to the Bragg grating entering a stage of plastic deformation beyond this range, deviating from the expected elastic behavior.

The sensitivity to tensile strain obtained from a linear fit of the experimental data is 100.6 με/mm, and -101.0 με/mm for compression strain, respectively.

For the case of the hollow device (Fig. 10B), the simulated data shows discrepancies with the experimental and simulated data starting from the 10 mm displacement. These discrepancies could be attributed to potential failures in the fabrication process of the structure with perforations, possibly leading to changes in the required perforation dimensions.

The sensitivity to tensile strain of the experimental data is 112.7 με/mm, and -101.3 με/mm for compression strain, respectively.

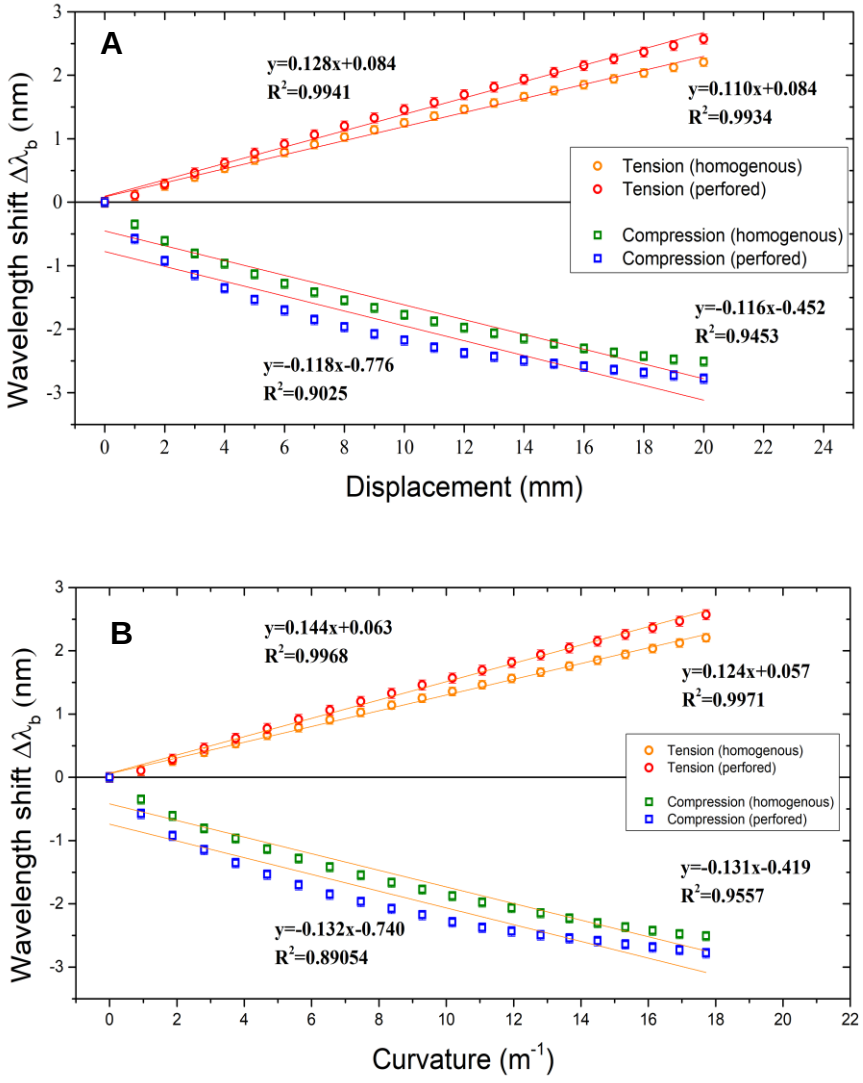

Fig. 10 Displacement and curvature response comparison for both devices in tension and compression states.

For the displacement sensitivities of both devices (Fig. 10A), there is an increase in sensitivity of 15% for the structure with perforations, with values of 128 pm/mm and 110 pm/mm for the homogeneous structure, respectively, in tensile strain. Similarly, for compressive strain, the sensitivities are -118 pm/mm and -116 pm/mm.

The same trend is observed for the sensitivity to the change in curvature of the sensor (Fig. 10B). A sensitivity of 124 pm/m^{-1} is presented for the solid device while the hollow device shows a higher sensitivity of 144 pm/m^{-1} in tensile strain. In the case of compression strain, both cases experience an increase in sensitivity, but linearity is lost throughout the measurement range, which spans from 0 to 20 mm.

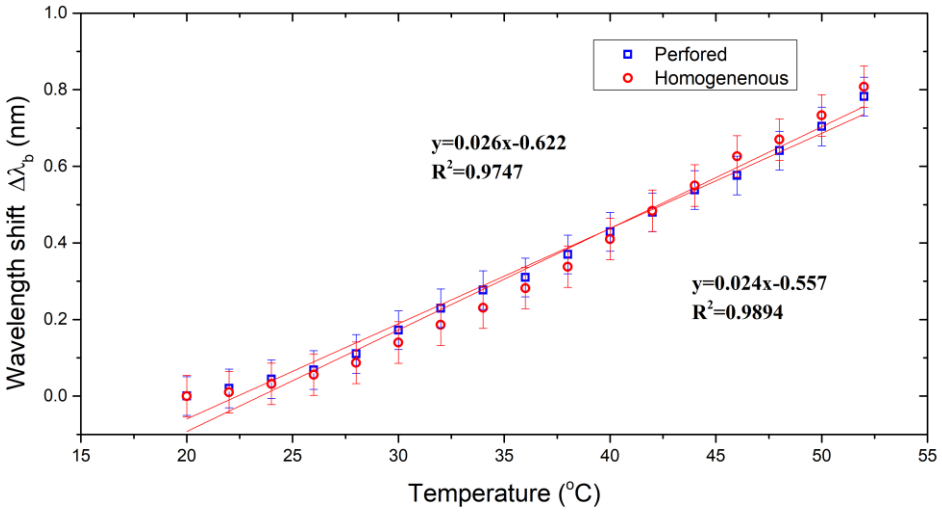

Fig. 11 Temperature response comparison between solid and hollow structures.

The response to temperature for both devices show sensitivities of 26 pm/°C for the homogeneous structure and 24 pm/°C for the perforated structure. This suggests that, initially, the perforations do not significantly modify the response to temperature changes, as expected.

6. CONCLUSIONS

The developed devices include a solid design and another with 3 central perforations, aimed at increasing sensitivity by concentrating efforts through these perforations.

The solid device exhibited a displacement sensitivity of 110 pm/mm, while the hollow device achieved a sensitivity of 128 pm/mm, representing a 15% increase. Both demonstrated high linearity with R^2=0.993 and R^2=0.994 respectively, within the displacement range of 0 to 20 mm in tensile strain configuration, and -116 pm/mm and -118 pm/mm in compression strain in the same displacement range.

In the case of sensitivity to curvature, the solid device presents a sensitivity of 124 pm/m^{-1} and the hollow device to 144 pm/m^{-1} with a linearity to R^2=0.997 and R^2=0.996

respectively in the tensile strain configuration and -131 pm/m^{-1} and -132 pm/m^{-1} in compression strain, with a reduction in the linearity factor, with values R^2=0.955 and R^2=0.890

Regarding temperature sensitivities, both devices showed remarkable values of 33 pm/°C and 34 pm/°C, respectively, considering the grating's embedded nature. To mitigate temperature effects, an additional grating can be incorporated using the temperature compensation method, a vital aspect of displacement monitoring.

These devices facilitate bidirectional displacement monitoring, responding to both tension and compression deformations of the grating. Furthermore, their sensitivity can be customized by adjusting the sensor's geometry to adapt to specific requirements of the displacement measurement required.

ACKNOWLEDGMENTS

The authors wish to acknowledge the financial support to Direccíon General de Asuntos de Personal Academico (DGAPA-UNAM) under the IT104123 project, the Master and Ph.D. Engineering Program (Programa de Maestría y Doctorado en Ingeniería) and the Instituto de Ciencias Aplicadas y Tecnología (ICAT) through the Universidad Nacional Autonoma de Mexico and Consejo Nacional de Humanidades Ciencias y Tecnología (CONAHCYT).

REFERENCES

Elsherif, M., Salih, A.E., Muñoz, M.G., Alam, F., AlQattan, B., Antonysamy, D.S., Zaki, M.F., Yetisen, A.K., Park, S., Wilkinson, T.D. and Butt, H. (2022), “Optical Fiber Sensors: Working Principle, Applications, and Limitations”. *Adv. Photonics Res., 3*: 2100371. https://doi.org/10.1002/adpr.202100371.

Mousumi Majumder, Tarun Kumar Gangopadhyay, Ashim Kumar Chakraborty, Kamal Dasgupta, D.K. Bhattacharya, (2008)” Fibre Bragg gratings in structural health monitoring—Present status and applications”, *Sensors and Actuators A: Physical*, 147(1), 150-164, https://doi.org/10.1016/j.sna.2008.04.008.

T. Bashir, A. Jalil, R. Rahman, (2006) “Fabrication of fiber grating by phase mask and its sensing application”, *J. Optoelectron. Adv. Mater.* **8** (4), 1841 - 7132. https://old.joam.inoe.ro/arhiva/pdf8_4/4Tahir.pdf.

M. Fajkus *et al*., (2020) "PDMS-FBG-Based Fiber Optic System for Traffic Monitoring in Urban Areas,” *IEEE Access*, **8,** 127648-127658, https://doi.org/10.1109/ACCESS.2020.3006985.

Morais, E.; Pontes, M.J.; Marques, C.; Leal-Junior, (2022) “A. Liquid Level Sensor with Two FBGs Embedded PDMS Diaphragm: Analysis of the Linearity and Sensitivity”. *Sensors* **22**, 1268. https://doi.org/10.3390/s22031268

Nedoma, J., Fajkus, M., Siska, P., Martínek, R., & Vasinek, V. (2017). “Non-invasive fiber optic probe encapsulated into Polydimethylsiloxane for measuring respiratory and heart rate of the human body.” *Advances in Electrical and Electronic Engineering,* **15**, 93-100. http://dx.doi.org/10.15598/aeee.v15i1.1923

F. Velazquez-Carreon, A. Perez-Alonzo, G.E. Sandoval-Romero, (2023)," Temperature-compensated fiber Bragg grating sensor based on curvature sensing for bidirectional displacements measurement", *Optical Fiber Technology,* **23,** 103257 https://doi.org/10.1016/j.yofte.2023.103257.

Qi Wang, Yu Liu, (2018) "Review of optical fiber bending/curvature sensor", *Measurement,* **130**, 161-176. https://doi.org/10.1016/j.measurement.2018.07.068.

Ariati R, Sales F, Souza A, Lima RA, Ribeiro J. (2021) "Polydimethylsiloxane Composites Characterization and Its Applications: A Review". *Polymers*, **13**(23), 4258. https://doi.org/10.3390%2Fpolym13234258

Lakshmanan, D., Kanakambaran, S. (2022). "Simulation Studies on Force Sensor Using PDMS Coated Fiber Bragg Grating for Robot-Assisted Surgery", *Optical and Wireless Technologies. Lecture Notes in Electrical Engineering,* **771**. 189-194. https://doi.org/10.1007/978-981-16-2818-4_20

Pilkey, W. D., & Pilkey, W. D. (2005). "Formulas for stress, strain, and structural matrices", *John Wiley & Sons***, 107,** 776-777.